Technical Report

TR-2008-009

A 3D/1D geometrical multiscale model of cerebral vasculature

by

Tiziano Passerini, Mariarita de Luca, Luca Formaggia, Alfio Quarteroni, Alessandro Veneziani

Mathematics and Computer Science

EMORY UNIVERSITY

A 3D/1D geometrical multiscale model of cerebral vasculature

Tiziano Passerini[1,2], Mariarita de Luca[1,3], Luca Formaggia[1], Alfio Quarteroni[1,4], Alessandro Veneziani[2]
1 *MOX, Dept. of Mathematics, Politecnico di Milano, Italy,* 2 *Dept. of Mathematics and Computer Science, Emory University, Atlanta, GA, USA* 3 *Dept. of Mech. Engr., University of Pittsburgh, Pittsburgh, PA, USA,* 4 *CMCS, EPFL Lausanne, Switzerland*

Abstract. Geometrical multiscale modeling is a strategy advocated in computational hemodynamics for representing in a single numerical model dynamics that involve different space scales. This approach is particularly useful to describe complex networks such as the circle of Willis in the cerebral vasculature. In this paper we present a multiscale model of the cerebral circulation where a one dimensional description of the circle of Willis, relying on the one-dimensional Euler equations, is coupled to a fully three dimensional model of a carotid artery, based on the solution of the incompressible Navier-Stokes equations. Even if vascular compliance is often not relevant to the meaningfulness of 3D results, it is crucial in the multiscale model, since it is the driving mechanism of pressure wave propagation. Unfortunately, 3D simulations in compliant domains still demand computational costs significantly higher than the rigid case. Appropriate matching conditions between the two models have been devised to concentrate the effects of the compliance at the interfaces and to obtain reliable results still solving a 3D problems on rigid vessels.

Keywords: Geometrical multiscale modeling, Circle of Willis, Domain splitting, Matching conditions

1. Introduction

The complexity of the vascular system demands for the set up of convenient mathematical and numerical models leading beyond usual models in fluid dynamics. Basically, computational hemodynamics relies on three classes of models, featuring a different level of detail in the space dependence.

Fully three dimensional models are based on the incompressible Navier-Stokes equations possibly coupled to appropriate models that describe the blood viscosity and the mechanical deformation of the vascular tissue. These models are well suited for investigating the effects of the geometry on the blood flow and the possible physio-pathological impact of hemodynamics. Unfortunately, the high computational costs restrict their use to contiguous vascular districts only on a space scale of few centimeters or fraction of meter at most (see e.g. (Cebral et al, 2003)).

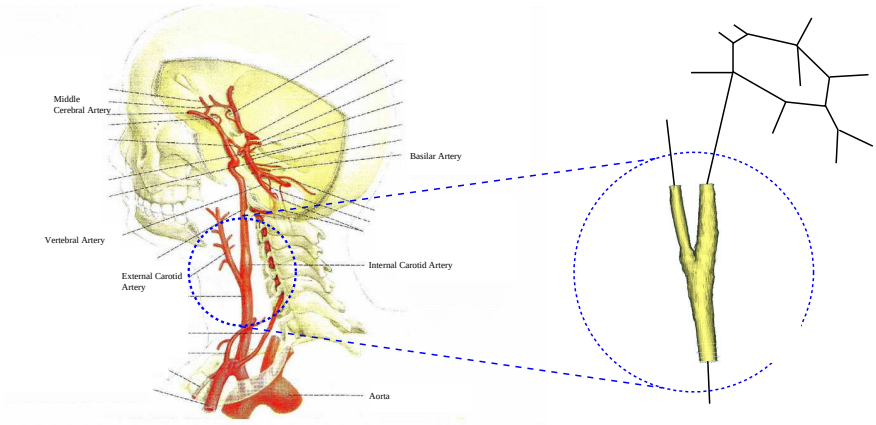

Figure 1. Left: Anatomical representation of the cerebral vasculature, including the circle of Willis (after (Balboni, 1993)). Right: Multiscale representation of the cerebral vasculature: a 3D representation of one of the carotid arteries is embedded in a 1D network of Euler problems

By exploiting the cylindrical geometry of vessels, it is possible to resort to *one-dimensional models*, by reducing the space dependence to the vessel axial coordinate only. These models are basically given by the well known Euler equations and provide an optimal tool for the analysis of wave propagation phenomena in the vascular system. They are convenient when the interest is on obtaining the pressure dynamics in a large part of the vascular tree at a reasonable computational cost (see (Peirò et al, 2008)). However, the space dependence still retained in these models inhibits their use for the whole vascular system. In fact, it would be unfeasible to follow the geometrical details of the whole capillary network.

A compartmental representation of the vascular system leads to a further simplification in the mathematical modeling, based on the *analogy between hydraulic networks and electrical circuits*. The fundamental ingredient of these *lumped parameter models* are the Kirchhoff laws, which lead to systems of differential-algebraic equations. These models can provide a representation of a large part or even the whole circulatory system, since they get rid of the explicit space dependence. They can include the presence of the heart, the venous system, and self-regulating and metabolic dynamics in a simple way and at a low computational cost.

All these models have peculiar mathematical features. They are able to capture different aspects of the circulatory systems that are however coupled together in reality. In fact, the intrinsic robustness

of the vascular system, still able to provide blood to districts affected by a vascular occlusion thanks to the development of compensatory dynamics, strongly relies upon this coupling of different space scales. Feedback mechanisms essential to the correct functioning of the vascular system work over the space scale of the entire network, even if they are activated by local phenomena such as an occlusion or the local demand of more oxygen by an organ. This is particularly evident in one of the most important parts of the vascular tree, the cerebral vasculature. Circulation in the head features a strongly coupled anastomotic system, called the *circle of Willis*, which ensures an adequate blood supply to the brain even when one of the incoming arteries is occluded or missing (see e.g. (Viedma et al, 1997; Alastruey et al, 2008)).

To devise numerical models able to cope with coupled dynamics ranging on different space scales a *geometrical multiscale approach* has been proposed in (Formaggia et al, 1999). Following this approach, the three different classes of models are mathematically coupled in a unique numerical model. Despite the intuitiveness of this approach, many difficulties arise when trying to combine numerically mathematical models that are self-consistent but not designed to work together. Some of these difficulties have been extensively discussed recently in (Quarteroni et al, 2008).

A practical difficulty arises when some features that could be neglected at a certain scale become essential in the coupled model, inducing a significant increase of the overall computational cost. This is the case of the compliance of vessels. In 3D Navier-Stokes standalone models compliance is quite often not relevant for bioengineering purposes. However, it is a driving mechanism of pressure wave propagation along the vascular tree. Therefore, when considering 3D/1D geometrical multiscale models in principle compliance should not be neglected in either models. The computational cost of a compliant 3D simulation is however by far higher than the rigid case. The coupling between 1D and 3D compliant models has been investigated recently in (Moura, 2007).

A naive coupling of the intrinsically compliant 1D model with a 3D rigid one, forcing for instance the continuity of pressure and flow rate at the interface, is problematic. The main reason is that the different mathematical modeling of the wall in the two subdomains cause spurious wave reflections at the interface between the models, strongly affecting the numerical results. We overcome these difficulties by resorting to appropriate matching conditions that mimic the presence of the compliance by concentrating it at the interface between the models. We introduce these conditions in Sect. 2. In Sect. 3 we present a multiscale model of the Willis circle based on a 1D network whose results are in

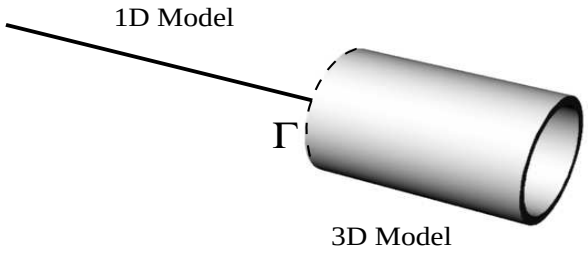

Figure 2. A simple multiscale (3D/1D) model of a cylindrical pipe

good agreement with results taken from the literature (Sect. 3.1). We illustrate multiscale simulations where a 3D model of the left carotid bifurcation is coupled with the 1D model of the Willis circle. Thanks to the adoption of matching conditions including the compliance it is possible to simulate the overall dynamics still solving a 3D rigid model, obtaining reliable results with relatively low CPU times.

2. Matching conditions in 3D rigid/1D multiscale models

To fix the ideas, let us refer to the simple model represented in Fig. 2. We assume that a cylindrical pipe has been split at section Γ into two halves. The left one is described in terms of the 1D Euler equations

$$\frac{\partial A}{\partial t} + \frac{\partial Q}{\partial x} = 0, \quad \frac{\partial Q}{\partial t} + \frac{\partial}{\partial x}\left(\alpha \frac{Q^2}{A}\right) + \frac{A}{\rho}\left(\frac{\partial P}{\partial x}\right) + K_R \frac{Q}{A} = 0. \qquad (1)$$

Here $A = A(t,x)$ represents the area of the vascular section at the abscissa x along the vessel axis and at time t, $Q = Q(t,x)$ is the corresponding flow rate, $P = P(t,x)$ is the pressure, ρ the blood density, α the so-called *momentum correction coefficient* and K_R a coefficient related to the viscosity of blood, see e.g. (Peirò et al, 2008) for more details. Area and pressure are related by the following algebraic wall law

$$P = P_{ext} + \frac{\sqrt{\pi} h_0 E}{(1-\nu^2)A_0}(\sqrt{A} - \sqrt{A_0}), \qquad (2)$$

where E is the Young modulus of the wall, h_0 is the wall thickness and ν the Poisson ratio. Hereafter the wall law is denoted by $P = \psi(A)$. The flow in the right hand side of the pipe is computed by the incompressible Navier-Stokes equations

$$\rho \frac{\partial \mathbf{u}}{\partial t} + \rho \mathbf{u} \cdot \nabla \mathbf{u} - \nabla \cdot (\mu \nabla \mathbf{u}) + \nabla p = \mathbf{0}, \quad \nabla \cdot \mathbf{u} = 0, \qquad (3)$$

where $\mathbf{u} = \mathbf{u}(x, y, z, t)$ is the velocity field, $p = p(x, y, z, t)$ the pressure, μ the blood viscosity.

Coupling the two models requires appropriate matching conditions. In the case of a rigid 3D model, it is reasonable to prescribe the continuity of pressure and the flow rate

$$P_{1D} = \frac{1}{|\Gamma|}\int_\Gamma p_{3D} d\gamma, \qquad Q_{1D} = -\rho \int_\Gamma \mathbf{u}_{3D} \cdot \mathbf{n} d\gamma, \tag{4}$$

where we have added the indexes $1D$ and $3D$ for the sake of clarity and denoted by $|\Gamma|$ the area of the interface Γ. The negative sign in the second of (4) stems from the fact that Q_{1D} and $\mathbf{u}_{3D}\cdot\mathbf{n}$ are directed outwards the 1D and 3D domains, respectively. In the sequel, for easiness of notation, we set $Q_{3D} = \rho \int_\Gamma \mathbf{u}_{3D} \cdot \mathbf{n} d\gamma$ and $P_{3D} = 1/|\Gamma| \int_\Gamma p_{3D} d\gamma$.

Other conditions can be considered as well, prescribing the continuity of the total pressure, of the normal stresses or of the characteristic variables (see (Quarteroni et al, 2008)).

When solving multiscale problems numerically it is natural to split the scheme into the iterative sequence of dimensionally homogeneous problems, which we indicate as 1D and 3D, for instance by means of the following algorithm. We assume that standard (Dirichlet or Neumann) conditions are prescribed at the boundaries of the overall 1D/3D model. Moreover, we carry out an appropriate space and time discretisation of the problems. In particular, apexes n and $n+1$ refer to the approximation of the solution at time steps t^n and t^{n+1} , respectively. Index k will refer to the inner iterations performed at a fixed time step, for the fulfillment of the matching conditions. For $n = 0, 1, \ldots$ we perform the following steps.

1) `Initialization.` Set $k = 0$, $\mathbf{u}_{3D,0}^{n+1} = \mathbf{u}_{3D}^n, p_{3D,0}^{n+1} = p_{3D}^n$ and $P_{1D,0}^{n+1} = P_{1D}^n$, $A_{1D,0} = \psi^{-1}(P_{1D,0}^{n+1})$, $Q_{1D,0}^{n+1} = Q_{1D}^n$.

2) `Loop.` on k

2.1)*Solve* the 1D model with the boundary condition on Γ given by

$$P_{1D,k+1}^{n+1} = \chi P_{3D,k}^{n+1} + (1-\chi) P_{1D,k}^{n+1}, \tag{5}$$

where χ is a relaxation parameter to be set for improving the convergence rate. Solving the 1D model, pressure conditions are recast in terms of area, thanks to the wall law $A_{1D,k+1}^{n+1} = \psi^{-1}(P_{1D,k+1}^{n+1})$.

2.2) *Solve* the 3D problem with the boundary conditions on Γ

$$Q_{3D,k+1} = -Q_{1D,k+1}^{n+1} \tag{6}$$

Set $k = k + 1$.

3) `Test.` Different convergence test can be pursued. A possibility is to check the continuity at the interface, namely terminate the iterations

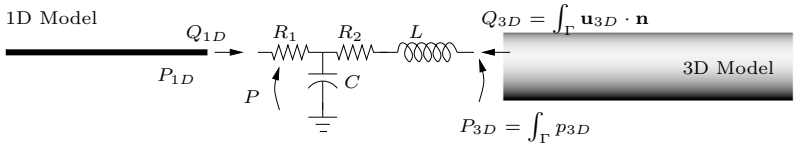

Figure 3. Representation of a multiscale with a 0D element representing the compliance of the 3D model at the interface.

when $|P^{n+1}_{1D,k+1} - P^{n+1}_{3D,k+1}| \leq \varepsilon$ being ε a user-defined tolerance. Another possibility is to check the residuals associated with the equations to be solved.

Swapping the role of the matching conditions in the set up of the boundary conditions for the iterative scheme, (5), (6) can be replaced by

$$Q^{n+1}_{1D,k+1} = -\chi Q^{n+1}_{3D,k} + (1-\chi) Q^{n+1}_{1D,k}, \qquad P^{n+1}_{3D,k+1} = P^{n+1}_{1D,k+1}. \tag{7}$$

The different space dependence of 1D and 3D models leads to unmatched or defective conditions (step 2 of the loop) and in particular (6) (or the second condition (7)) do not prescribe sufficient conditions for the closure of the Navier-Stokes problem. The latter needs to be solved in the framework of *defective boundary problems*, being the data available at the boundary not enough to guarantee the uniqueness of the solution. This topic has been discussed in (Quarteroni et al, 2008), Chap.11, where different mathematically sound techniques for the solution of defective problems are presented. The specific method for solving the 3D problem affects the accuracy of the Navier-Stokes solution and is not relevant for the purpose of the present paper, so we do not dwell upon it. Any reasonable technique can be used in the context of our multiscale modeling.

The iterative approach given by the previous three steps suffers from numerical problems induced by the different description of the wall mechanics in the two halves of the pipe, which produces spurious reflections at the interface and possible numerical instabilities. One could avoid this kind of problems by resorting to a compliant 3D model. As we have pointed out, this increases the computational costs strongly. In the next subsection, we present a different strategy based on the set up of an appropriate set of interface conditions.

2.1. Matching conditions including compliance

2.1.1. *A simple case*

Suppose to give a simplified representation of the compliance of the 3D vessel in the multiscale model, by gathering its effect at the interface using a special lumped parameter model. Referring for instance to Fig. 3, we introduce a *RCL network* at the interface with the role of representing the effects of the compliance of the artery in the 3D model. In this way, we still use a 3D rigid model, which however behaves like a compliant one with respect to the system dynamics. By denoting with P the pressure associated with the capacitance C, we can derive the following set of equations,

$$P = P_{1D} - R_1 Q_{1D},\ P = P_{3D} - L\frac{dQ_{3D}}{dt} - R_2 Q_{3D},\ C\frac{dP}{dt} = Q_{1D} + Q_{3D}. \tag{8}$$

Taking the derivative of the first equation and using the third, we can eliminate P and finally obtain the new conditions in the iterative scheme, by replacing (5) and (6) with

$$\begin{aligned} P_{1D,k+1} &= \chi\left(P_{3D,k} - L_1\frac{dQ_{3D,k}}{dt} - R_2 Q_{3D,k} + R_1 C_1\frac{dP_{3D,k}}{dt}\right. \\ &\left. -R_1 C L\frac{d^2 Q_{3D,k}}{dt^2} - R_1 C R_2\frac{dQ_{3D,k}}{dt} - R_1 Q_{3D,k}\right) + (1-\chi)P_{1D,k} \\ Q_{3D,k+1} &= -Q_{1D,k+1} + C\frac{dP_{1D,k+1}}{dt} - R_1 C\frac{dQ_{1D,k+1}}{dt} \end{aligned} \tag{9}$$

These conditions (hereafter denoted by *LP* (Lumped Parameter) *conditions*) involve time derivatives of the matching quantities. They have been discretized with finite differences of the same accuracy of the time advancing scheme used for the time discretisation of the Navier-Stokes and Euler equations. More precisely, in this work we resorted to the first order implicit finite differences.

Remark As expected, for $C = 0$, $R_1 = R_2 = 0$ and $L = 0$ we recover the coupling given by conditions (5), (6). This corresponds physically to the case of a rigid portion of artery in a network of compliant vessels, as it is the case of a stented or prosthetic segment (see (Lamponi et al, 2003)).

Parameters estimation The interface LP model of Fig. 3 provides a physical representation to our matching conditions. In particular, we resorted to a classical RCL network, so far advocated for representing the capillary circulation (see (Stergiopulos at al, 1999; Alastruey et al, 2008)).

Following classical arguments for the derivation of lumped parameter models (see e.g. (Quarteroni et al, 2008) Chap. 10) we remind that for a cylindrical vessel with length l, area A_0, with a linear elastic wall with thickness h_0 and Young modulus E the compliance may be estimated to be $C \propto \dfrac{A_0^{3/2} l}{E h_0}$. Physiological values of this parameter are of the order of 10^{-5} cm^5/dyn. In our computation ($l = 5$ cm and $A_0 = \pi$ cm^2) we set $C = 5.8910^{-5}$ cm^5/dyn. The other parameters have been properly adjusted in order to reduce spurious effects at the 1D/3D interfaces. More precisely, resistance R_1 is fixed as suggested in (Alastruey et al, 2007) so that an incoming wave from the 1D model is propagated without any reflection. Resistance R_2 and L have been set after some numerical experiments to $R_2 = 1$ dyn s cm^{-2} and $L = 0.01$ g cm$^-4$.

The impact of the LP conditions is illustrated in Fig. 4 and 5. More precisely, in Fig. 4 we illustrate results obtained for the model of Fig. 3 when a sinusoidal waveform for the flow rate is prescribed at the inlet. We compare the time history of the flow rate and area (as function of the pressure) at the interface, denoted by Q_{1D} and $A(P_{1D})$ in Fig. 3, obtained with a standard multiscale 1D/3D model , using the proposed approach and finally those obtained with a complete 1D model. In Fig. 5 we present similar comparisons for the case when a step waveform is prescribed at the inlet of the domain. The impact of interface conditions is evident. In the case based on classical matching, the solution is dramatically affected by reflections induced by the different description of the wall mechanics in the 1D and 3D model. These reflections change completely the profile of the solution. On the other side, matching conditions based on the RCL model are able to obtain a behavior similar to that of the complete 1D model, even if we are using a rigid 3D model. The same conclusions hold for the area: the RCL-based conditions allow us to find a solution significantly close to that of the complete 1D model. We point out that a proper tuning of the parameters is crucial to find the best RCL model.

2.2. A 1D-3D-1D coupling

Let us consider now the case represented in Fig. 6, where we show a sequence of 1D-3D-1D model with appropriate LP conditions. From the numerical point of view on the left interface we still resort to the iterative scheme with conditions (9). On the right interface, we adopt a similar iterative strategy where we prescribe a pressure condition to the 3D problem and flow rate conditions to the 1D Euler system downstream. More precisely, equations corresponding to the downstream

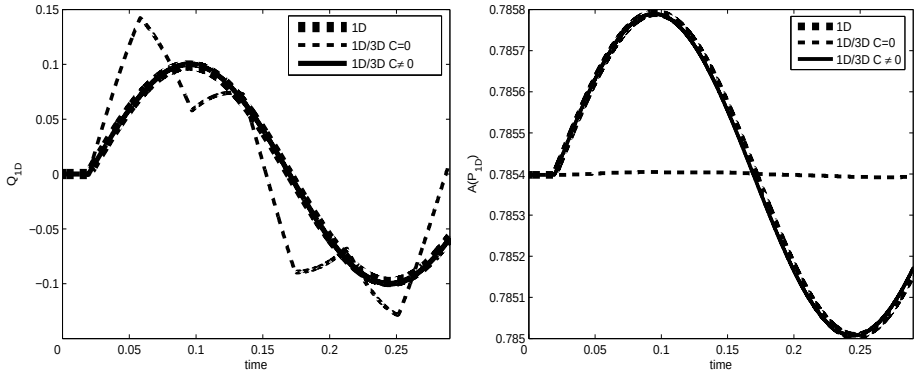

Figure 4. Comparison of dynamics of flow rate (left) and area (right) at $x = 5cm$ of a compliant pipe simulated with a fully 1D model, a multiscale 1D/3D model with direct coupling and with the matching conditions obtained by the lumped parameter models. The input waveform of the flow rate at the tube inlet is a sine with amplitude 0.1.

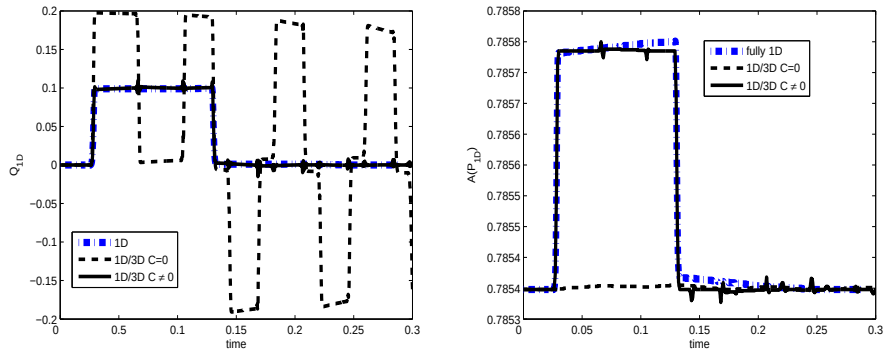

Figure 5. Comparison of dynamics of flow rate (left) and area (right) at $x = 5cm$ of a compliant pipe simulated with a fully 1D model, a multiscale 1D/3D model with direct coupling and with the matching conditions obtained by the lumped parameter models. The input waveform of the flow rate at the tube inlet is a step function with amplitude 0.1.

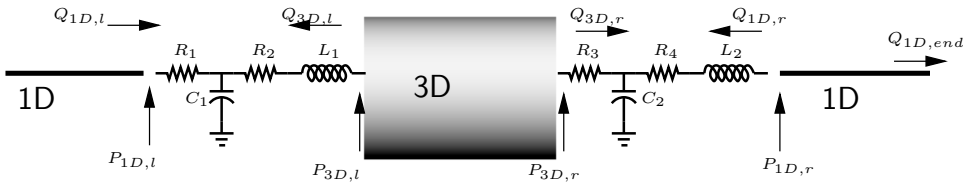

Figure 6. Representation of a multiscale model with a two buffer 0D elements at the interface.

interface read

$$\begin{cases} P_{3D} - R_3 Q_{3D} = P_{1D} - L_2 \dfrac{dQ_{1D}}{dt} - R_4 Q_{1D} \\ C_2 \dfrac{dP_{3D}}{dt} - R_3 C_2 \dfrac{dQ_{3D}}{dt} = Q_{1D} + Q_{3D} \end{cases}$$

Consequently, the coupling conditions used in the iterative scheme are

$$\begin{cases} Q_{1D,k+1} = \chi \left(-Q_{3D,k} + C_2 \dfrac{dP_{3D,k}}{dt} - R_3 C_2 \dfrac{dQ_{3D,k}}{dt} \right) + (1-\chi) Q_{1D,k} \\ P_{3D,k+1} = P_{1D,k+1} - L_2 \dfrac{dQ_{1D,k+1}}{dt} - R_4 Q_{1D,k+1} + R_3 C_2 \dfrac{dP_{1D,k+1}}{dt} - \\ \qquad R_3 C_2 L_2 \dfrac{d^2 Q_{1D,k+1}}{dt^2} - R_3 C R_4 \dfrac{dQ_{1D,k+1}}{dt} - R_3 Q_{1D,k+1} \end{cases} \tag{10}$$

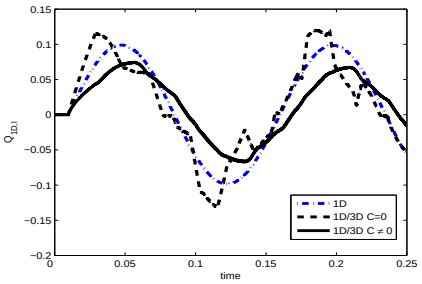

Numerical results are reported in Fig. 7. Again, we illustrate the comparison of the solutions obtained with a 1D model, and the multiscale models corresponding to Fig. 6, where all the lumped parameters are null (classical conditions) and when they are activated. The inlet waveform is sinusoidal.

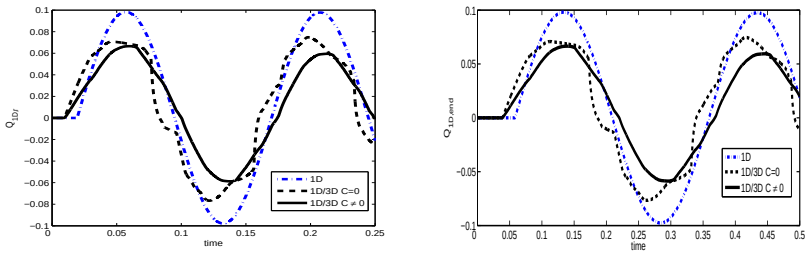

Figure 7. Comparison of flow rates computed by a 1D (dash-dot line), a multiscale 1D/3D/1D model with classical matching conditions (dashed line) and with lumped parameter matching conditions (solid line) in correspondence of the first interface (top), the second (bottom, left) and the outlet of the domain (bottom, right).

In the first picture we present the flow rate at the first interface (denominated $Q_{1D,l}$ in Fig. 6) in the second picture the flow rate $-Q_{1D,r}$ at the second interface and finally the flow rate $Q_{1D,end}$ at the outlet of the right pipe. Again, when classical matching conditions are used

(corresponding to null values of the parameters) the superimposition of the components induced by reflections triggered by the different wall models is evident. This changes the shape of the propagating wave and affects both the amplitude and the phase. Amplitude dissipation in the forward component of the wave is partially compensated by the superimposition of the spurious reflections. In the case of LP conditions, the shape of the wave is only partially affected. Dispersion errors are remarkably small, whilst dissipation effects are present. The impact of finite difference schemes in the numerical implementation of matching conditions is probably the main responsible of these effects. A more accurate analysis of this aspect will be carried out elsewhere. Matching conditions guarantee in any case a significant reduction of spurious reflections.

3. Multiscale model of the circle of Willis

The Willis circle is the main collateral pathway of the cerebral circulation. It is essentially given by a polygonal ring at the basis of the brain . The polygon (see Fig. 8) is made of the right and left Posterior Cerebral Arteries (rPCA and lPCA), the right and left Posterior Communicating Arteries (rPCoA and lPCoA), the right and left Anterior Cerebral Arteries (rACA and lACA) and the Anterior Communicating Artery (ACoA). Blood is supplied by the two Internal Carotid Arteries (rICA and lICA) and the two Vertebral Arteries (rVA and lVA). The latter joins into the Basilar Artery (BA), from which the two PCAs depart, delivering blood in the posterior region of the brain. The two ACAs depart from the ICAs and deliver blood to the anterior part of the brain. This complex structure has two advantages. On the one hand it supplies blood to the brain even when one or more vessels are occluded or missing. On the other hand, it protects the brain from not uniform or excess supply of blood, distributing it uniformly.

It is well known that in fact in almost 50 % of the population one of the branches of the circle is absent or partially developed (Lippert and Pabst, 1985). A correct knowledge of the functioning of the circle of Willis is relevant in clinical practice for many intracranial or extracranial procedures like endoarterectomy, carotid stenting or the compression carotid test (see e.g. (Hetze et al., 2000)). Several mathematical studies have been carried out for devising quantitative analysis of this district. After the first studies based on hydraulic or electric analog models (Rogers, 1947; Avman et al, 1961; Murray, 1964; Fasano et al, 1966), we mention the investigations carried out in (Clark et al, 1967). Most of the research is based on modeling the circle of Willis

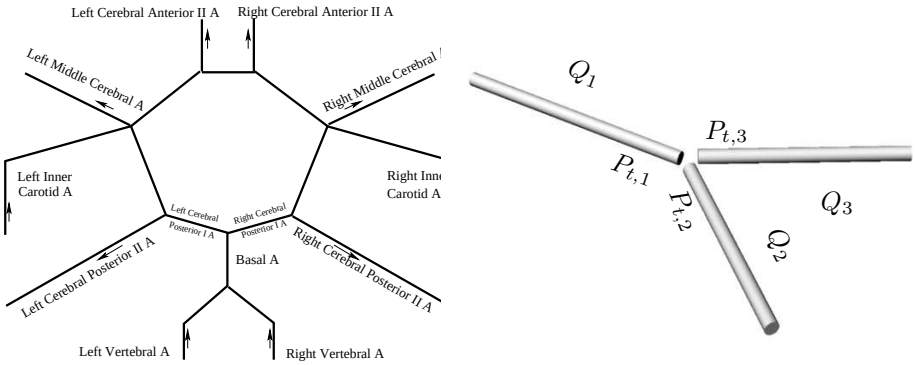

Figure 8. 1D model of the circle of Willis: description of the circle (left) and a bifurcation (right).

as a set of 1D Euler problems (1), representing each branch of the circle, with an appropriate modeling of the bifurcations. Among the others, we mention (Hillen, 1986; Hillen at al, 1988; Lyden and Nelson, 1997; Macchi et al, 1996; Viedma et al, 1997; David et al, 2003; Alastruey et al, 2008). More recently, metabolic models have been added to simulate cerebral auto-regulation, which is a feedback mechanism driving an appropriate blood supply into the circle on the basis of oxygen demand by the brain (Alastruey et al, 2007). A complete 3D image based numerical model of the circle of Willis has been presented in (Cebral et al, 2003). It requires medical data that are currently beyond the usual availability in common practice, and is computationally intensive. Hereafter, we propose a multiscale model where the 3D simulation is used only in the region of interest (the left ICA in our case) and the remainder of the network is modeled by a 1D network. A similar multiscale model has been investigated in (Moura, 2007), where the 3D model includes compliance for avoiding spurious reflections induced by a rigid treatment of the 3D geometry in the multiscale model. Here we compare and discuss results obtained with a rigid model and the lumped-compliance matching conditions just described.

3.1. The 1D network

In our model, the Wills circle is represented by an oriented graph. The edges of the graph correspond to the vessels, while the nodes are the junctions. Each edge (see Fig. 8 on the left) has been described by system (1) where appropriate initial conditions have been assumed. The junctions have been modeled by prescribing balance equations for the mass and the total pressure $P_t = P + 1/2\rho U^2$ (see (Lamponi et al, 2003; Matthys et al, 2007)). For the sake of concreteness, if we refer to

Table I. Flow distribution in Anterior Cerebral Artery, Middle Cerebral Artery and Posterior Cerebral Artery computed in different models proposed in the literature and in the present one

Model	ACA %	MCA %	PCA %
Hillen (Hillen, 1986)	22.2	45.0	32.8
Hillen (Hillen at al, 1988)	22.1	44.8	33.1
Lyden (Lyden and Nelson, 1997)	21.2	53.6	25.2
Macchi (Macchi et al, 1996)	23.2	53.4	42.4
Viedma (Viedma et al, 1997)	24.5	49.9	27.8
Ferrandez (David et al, 2003)	22.3	49.9	34.9
Our model	20.8	44.9	34.3

Fig. 8 on the right, we will prescribe

$$Q_1 + Q_2 + Q_3 = 0, \begin{array}{l} P_{1,t} = P_{2,t} + \varphi(U, \alpha_{12}) \\ P_{1,t} = P_{3,t} + \varphi(U, \alpha_{13}) \end{array}$$

where functions φ possibly include some dissipation effects depending on the bifurcation angles. We assume $\varphi = 0$, since the numerical solution has been proved to be weakly affected by this choice (see (Lamponi et al, 2003)).

The inlets of the system are placed in correspondence of the 1D models representing the CCAs and the VAs (see Fig. 1). We impose on the first $310^{?3}$ seconds a flux impulse of $6.8cm^3/s$ on each vertebral artery, and of $12.75cm^3/s$ on the right internal carotid artery, setting the flux value to zero after that. In the left internal carotid artery, represented by the 1D model upstream the 3D model, we assume to prescribe an inlet waveform given by the sinusoidal function $16.3\sin(\pi t/T)$ for $0 < t \leq T$, with $T = 6e^{-3}$, and 0 elsewhere.

At the outlet of the network we prescribe absorbing boundary conditions. More complex conditions, including a three elements Windkessel model for the peripheral circulation has been proposed in (Matthys et al, 2007) and can be integrated easily in our approach.

To validate our code we have reported in Tab. I the distribution of fluxes obtained by models of the Willis circle available in the literature and our results. The agreement is rather good.

3.2. The 3D carotid model and the multiscale coupling

The multiscale model is depicted in Fig. 1, on the right. The geometry of the Left Internal Carotid geometry is based on the realistic model by Liepsch, see (Prosi et al., 2005). The Navier-Stokes equations in the

3D model have been solved with the code LifeV - see `www.lifev.org` - based on a $P1P1$ finite element solver stabilized by means of an interior penalty approach. At the interfaces between the 3D and 1D models we prescribe conditions (9) at the upstream interface and conditions (10) at the downstream interfaces.

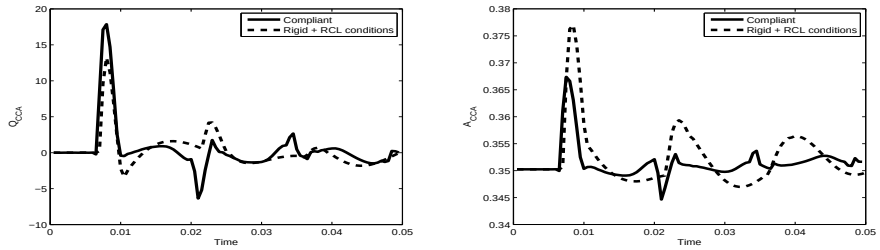

Figure 9. Comparison of the results obtained with the 3D compliant (solid line) and the 3D rigid with RCL conditions at the inlet of Common Carotid Artery (dashed line). Left: flow rate, Right: Area.

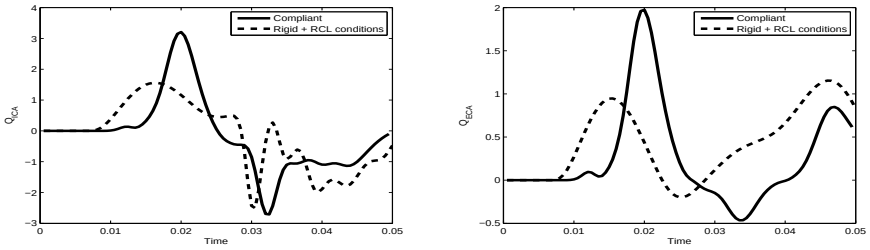

Figure 10. Comparison of the results obtained with the 3D compliant (solid line) and the 3D rigid with RCL conditions in the branches. Artery (dashed line). Left: flow rate at the internal carotid, Right: flow rate at the external carotid.

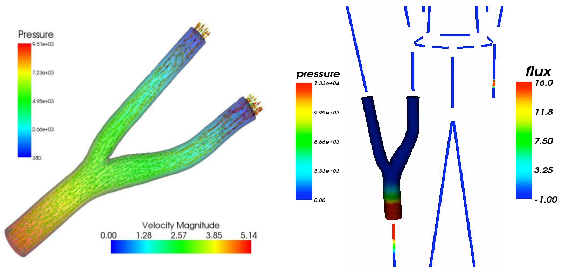

Figure 11. Left: Representation of the 3D solution (velocity and pressure). Right: Coupling of 3D and 1D computations.

In Fig. 9, Fig. 10 and Fig. 11 we present the results, in comparison with the ones of the compliant multiscale model presented in (Moura,

2007). Results underline that the RCL based conditions can actually obtain good solutions, in particular at the inlet. At the outlets of the carotid arteries the solution seems to be strongly dissipated even if phase error is quite small. Impact of the time discretisation of the matching conditions and the selection of the parameters on the dissipation error is under investigation.

Fig. 11 illustrates velocity and pressure fields in the 3D rigid model. On the left we present a detail of the 3D velocity field, on the right a multiscale perspective coupling local and global dynamics.

Acknowledgments A. Quarteroni, L. Formaggia and A. Veneziani are supported by the Project "Mathematical and numerical modelling of the electro-fluid-mechanics of the Heart" granted by the National Institute of High Mathematics (INDAM), Italy. T. Passerini, M. de Luca and A. Veneziani are supported by the Project Aneurisk, granted by Fondazione Politecnico di Milano and SIEMENS Medical Solutions, Italy.

References

Balboni, G. Anatomia Umana 1. *Ediz. Ermes*

Quarteroni A. Formaggia L. and Veneziani A., *Multiscale models of the vascular system*, Chapter 11 of Quarteroni, A. and L. Formaggia and A. Veneziani (eds.) *Cardiovascular Mathematics* Springer NY, to appear

Peirò J and Veneziani A., *Reduced models of the cardiovascular system*, Chapter 10 of Quarteroni, A. and L. Formaggia and A. Veneziani (eds.) *Cardiovascular Mathematics* Springer NY, to appear

Alastruey J, Parker KH, Peirò J, Byrd SM, Sherwin SJ. *Modelling the circle of Willis to assess the effects of anatomical variations and occlusions on cerebral flows.* Journal of Biomechanics 2007;40:1794-1805

Alastruey J, Moore SM, Parker KH, David T, Peirò J, Sherwin SJ. *Reduced modelling of blood flow in the cerebral circulation: coupling 1D, 0-D and cerebral autoregulation models.* Int J Num Meth Fl 2008;56:1061-1067

Avman N, Bering EA. *A plastic model for the study of pressure changes in the circle of Willis and major cerebral arteries following arterial occlusion.* Journal of Neurosurgery 1961;18:361-365

Cebral JR, Castro MA, Soto O, Lohner R, Alperin N. *Blood-flow models of the circle of Willis from magnetic resonance data.* Journal of Engineering Mathematics 2003;47:369-386

Clark ME, Himwich WA, Martin JD. *Simulation studies of factors influencing cerebral circulation.* Acta Neurologica Scandinavica 1967;43:189

Clark ME, Himwich WA, Martin JD. *A comparative examination of cerebral circulation models.* Journal of Neurosurgery 1968;29:484

Clark ME, Martin JD, Wenglarz RA, Himwich WA, Knapp FM. *Engineering analysis of the hemodynamics of the circle of Willis.* Archives of Neurology 1965;13:173

David T, Brown M, Ferrandez A. *Auto-regulation and blood flow in the cerebral circulation.* International Journal for Numerical Methods in Fluids 2003;43:701-713

Fasano VA, Broggi G. *Discussion sur le polygone de Willis.* Neurochirurgie 1966;12:761

Hillen B. *The variability of the circle of Willis - Univariate and bivariate analysis.* Acta Morphologica Neerlando-Scandinavica 1986;24:87-101

Hillen B. *On the meaning of the variability of the circle of Willis.* Acta Morphologica Neerlando-Scandinavica 1986;24:79-80

Hillen B, Drinkenburg BAH, Hoogstraten HW, Post L. *Analysis of flow and vascular resistance in a model of the circle of Willis.* Journal of Biomechanics 1988;21:807-814

Hillen B, Hoogstraten HW, Post L. *A mathematical model of the flow in the circle of Willis.* Journal of Biomechanics 1986;19:187-194

Macchi C, Catini C, Federico C, et al. *Magnetic resonance angiographic evaluation of circulus arteriosus cerebri (circle of Willis): a morphology study in 100 human healthy subjects.* Italian Journal of Anatomy and Embryology 1996;101:115-123

Matthys KS, Alastruey J, Peirò J, Khir AW, Segers P, Verdonck PR, Parker KH, Sherwin SJ, *Pulse wave propagation in a model human arterial network: Assessment of 1-D numerical simulations against in vitro measurements.* Journal of Biomechanics 2007;40:3476-3486

Murray KD. *Dimensions of circle of Willis and dynamic studies using electrical analogy.* Journal of Neurosurgery 1964;21:26

Rogers L. *The function of the circulus arteriosus of Willis.* Brain 1947;70:171-178

Viedma A, Jimenez Ortiz C, Marco V. *Extended Willis circle model to explain clinical observations in periorbital arterial flow.* Journal of Biomechanics 1997;30:265-272

Formaggia L., Nobile F., Quarteroni A., Veneziani A., *Multiscale modelling of the circulatory system: a preliminary analysis*, Comput. Visual. Sci. 1999; 2(2/3):75-83

Moura A., *The geometrical multiscale modelling of the cardiovascular system: coupling 3D FSI and 1D models*, Mox PhD Thesis, Dept. of Mathematics, Politecnico di Milano, Italy, 2007

Formaggia, L., Lamponi, D., Quarteroni, A., *One-dimensional models for blood flow in arteries*, J. Engrg. Math., 2003; 47, 251-276

Stergiopulos N., Westerhof B.E., Westerhof N., *Total arterial inertance as the fourth element of the Windkessel model*, Am. J. Physiol., 1999; 276, H81-H88

Lippert H., Pabst R., *Arterial variations in man: classification and frequency.* JF. Bergmann, Munich, 1985

Hetzel A., von Reuternc G.-M., Wernza M.G., Drostea D.W., Schumacher M., *The carotid compression test for therapeutic occlusion of the internal carotid artery* Cerebrovasc Dis 2000;10:194-199

P. Lyden and T. Nelson, *Visualization of the cerebral circulation using three dimensional transcranial power Doppler ultrasound imaging,* J Neuroimag 1997, 7:35-39

M Prosi, P Zunino, K Perktold, A Quarteroni, *Mathematical and numerical models for transfer of low-density lipoproteins through the arterial walls: a new methodology for the model set up with applications to the study of disturbed lumenal flow.* J J Biomech. 2005;38 (4):903-17

Taylor CA, Hughes TJ, Zarins CK, *Finite element modeling of three-dimensional pulsatile flow in the abdominal aorta: relevance to atherosclerosis.* Ann Biomed Eng 1998 Nov-Dec; 26 (6): 975-87